J|A|C|S
ARTICLES
Published on Web 01/06/2006

Competition between Metal-Amido and Metal-Imido Chemistries in the Alkaline Earth Series: An Experimental and Theoretical Study of BaNH

Alexandra Janczyk, Dennis L. Lichtenberger, and Lucy M. Ziurys*

Contribution from the Departments of Chemistry and Astronomy, The University of Arizona, Tucson, Arizona 85721

Received May 27, 2005; E-mail: lziurys@as.arizona.edu

Abstract: The pure rotational spectrum of BaNH in its $X^1\Sigma^+$ ground electronic state has been recorded using millimeter/submillimeter direct absorption methods; data for the deuterium and barium 137 isotopomers have been measured as well. The molecules were produced by the reaction of ammonia or ND_3 and barium vapor in the presence of a dc discharge. Transitions arising from the ground vibrational state and the excited vibrational bending (01^10) and heavy atom stretching (100) modes were measured. The rotational spectrum indicates a linear structure, with B_0(BaNH) = 7984.549 MHz and B_0(BaND) = 7060.446 MHz. An $r_m^{(1)}$ structure has been determined, yielding r(BaN) = 2.077 ± 0.002 Å and r(NH) = 1.0116 ± 0.0006 Å. Density functional calculations using an extensive Slater-type basis set with inclusion of scalar relativistic effects gives geometrical parameters and vibrational frequencies for BaNH in excellent agreement with those determined by experiment. The molecular orbital and natural bond order analyses of the BaNH wave function show Ba−N π bonds formed by electron donation from the formally filled N 2p orbitals of the imido group to the empty Ba 5d orbitals. The multiple bonding between Ba and N stabilizes the linear geometry and, along with the relative ease of oxidation of the Ba atom, favors formation of the metal-imido species over that of the metal-amido species that have been found from similar studies with Mg, Ca, and Sr atoms in this group.

Introduction

Metal-amine, -amido, and -imido species play central roles in many important chemical processes and developing materials applications.[1,2] For processes proceeding from amines to metal-imidos, these species represent successive steps in nitrogen−hydrogen bond activation, and for processes proceeding in the opposite direction, they represent successive steps in reduction of nitrogen to ammonia. Aside from these relationships, metal-amido and metal-imido complexes can serve as reagents for chemical processes such as carbon−nitrogen bond forming reactions and carbon−hydrogen bond activation or precursors for metal-nitrides and other materials. Alkali and alkaline earth metal-amido and -imido species have recently been proposed as materials for storage of hydrogen.[3] An understanding of the factors that determine the structures, bonding, and relative stabilities of metal-amine, -amido, and -imido species, as well as the mechanisms for formation and interconversion of these species, is an important step to developing the chemistry and applications of metals with nitrogen-containing species.

The alkali and alkaline earth metals offer an opportunity to study these species in detail in the absence of other ligands bound to the metal and with well-defined geometric and electronic structures. Gas-phase spectroscopy studies to this point have suggested that both alkali and alkaline earth metals preferentially form the amide species MNH_2 on reacting with ammonia in a dc discharge.[4−8] For example, both $NaNH_2$ and $LiNH_2$ have been successfully produced in the gas phase, and their rotational spectra have shown that these are planar species with a $^1A_1$ ground electronic state.[4,5] Magnesium, calcium, and strontium amides have been investigated as well, by both optical and pure rotational spectroscopy.[6−10] These molecules have proven to be radicals with $^2A_1$ ground electronic states; i.e., they are planar with C_{2v} symmetry. Another possible geometry for the amides is pyramidal; however such structures have not been found for these species. The bonding in these molecules has been interpreted to be more ionic than covalent.[6]

Not all metals create amides on reaction with ammonia. Several transition metals, for example, scandium and yttrium,

(1) Wigley, D. E. *Prog. Inorg. Chem.* **1994**, *42*, 239.
(2) Chisholm, M. H.; Rothwell, I. P. Amido and Imido Metal Complexes. In *Comprehensive Coordination Chemistry*; Wilkenson G., Gillard, R. D., McCleverty, J. A. Eds.; Pergamon: Oxford, U.K., 1987; Vol. 2, p 161.
(3) (a) Meisner, G. P.; Pinkerton, F. E.; Meyer, M. S.; Balogh, M. P.; Kundrat, M. D. Imide/amide hydrogen storage system. U.S. Patent Application 20040265226, 2004; *SciFinder Scholar* AN 2005:976. (b) Nakamori, Y.; Kitahara, G.; Orimo, S. *J. Power Sources* **2004**, *138*, 309. (c) Chen, P.; Xiong, Z.; Luo, J.; Lin, J.; Tan, K. L. *Nature* **2002**, *420*, 302.
(4) Grotjahn, D. B.; Sheridan, P. M.; Jihad, I. A.; Ziurys, L. M. *J. Am. Chem. Soc.* **2001**, *123*, 5489.
(5) Xin J.; Brewster, M. A.; Ziurys, L. M. *Astrophys. J.* **2000**, *530*, 323.
(6) Sheridan, P. M.; Ziurys, L. M. *Can. J. Phys.* **2001**, *79*, 409.
(7) Brewster, M. A.; Ziurys, L. M. *J. Chem. Phys.* **2000**, *113*, 3141.
(8) Thompsen, J. M.; Sheridan, P. M.; Ziurys, L. M. *Chem. Phys. Lett.* **2000**, *330*, 373.
(9) Bopegedera, A. M.; Brazier, C. R.; Bernath, P. F. *J. Phys. Chem.* **1987**, *91*, 2779.
(10) Whitham, C. J.; Jungen, C. *J. Chem. Phys.* **1990**, *93*, 1001.

have been found to preferentially form the linear imide species MNH.[11−15] Studies of the $A^2\Pi_r-X^2\Sigma^+$ transition of ScNH by Steimle and co-workers have shown that this species is linear.[11] Simard and collaborators detected the $B^2\Sigma-\tilde{X}^2\Sigma$, $\tilde{A}^2\Pi-\tilde{X}^2\Sigma^+$ and $\tilde{X}''^2\Pi_{1/2}-\tilde{X}^2\Sigma$ systems of YNH, confirming that the molecule is linear in the ground and several excited electronic states.[12−14] The $\tilde{B}^2\Sigma^+-\tilde{X}^2\Sigma^+$ transition of LaNH has been observed by Merer and co-workers;[15] again, a linear structure was found for this species as well.

In our laboratory, we have been recording the pure rotational spectra of metal-containing amide molecules, including the alkaline earth species $MgNH_2$, $CaNH_2$, and $SrNH_2$.[6−8] To complete the alkaline earth series, we began an investigation of the pure rotational spectrum of $BaNH_2$, using our usual amide synthetic technique of reacting ammonia with metal vapor in a dc discharge. Instead of producing $BaNH_2$, linear BaNH was formed, as indicated by the rotational pattern observed. These data suggest that the bonding in barium differs from that of the lighter alkaline earth metals. Density functional calculations were carried out to investigate the electronic structure and bonding of BaNH. The results agree with the linear structure and bond lengths of BaNH determined experimentally, and analysis of the wave function shows that the virtual 5d orbitals of barium participate in π bonding with the 2p orbitals of nitrogen. This property has been suggested by previous theoretical studies of CsNBa.[16] In addition to the availability of the Ba 5d orbitals for σ and π bonding, the low ionization energy of the valence Ba 6s orbital (occupied for the neutral atom) and the relative ease of oxidation of the barium atom appear to favor the formation of the metal-imido species from the reaction of barium with ammonia in the dc discharge, in contrast to the formation of the metal-amido species for the lighter metals in this group. In this paper we present our BaNH rotational spectra and their analysis, the BaNH structure, and our computational study of the bonding, structure, and mechanism of formation of the group II metal-amido and -imido species.

Experimental Section

Rotational Spectroscopy. The rotational spectrum of BaNH and three of its isotopomers were measured using one of the millimeter wave spectrometers of the Ziurys group.[17] The source of radiation consists of phase-locked Gunn oscillators combined with Schottky diode multipliers, which enables a frequency coverage of 65−640 GHz. The microwave radiation propagates quasi-optically through the reaction cell, a double pass system, using a series of Teflon lenses, a wire grid, and a rooftop reflector. The radiation is detected by a helium-cooled InSb hot electron bolometer.

BaNH was created by a reaction of barium metal with NH_3 in the presence of a dc discharge. Barium vapor was produced by a Broida-type oven, as described previously.[18] 3 mTorr of NH_3 were introduced to the cell through a tube located above the oven, while 20−25 mTorr of argon were introduced from below the oven in order to stabilize the discharge. To synthesize BaND, 3 mTorr of ND_3 (Cambridge laboratories) were used instead. The dc discharge was run at 20−50 V and 200−500 mA and was found essential to synthesize the molecule. To obtain the desired BaNH lines, the oven temperature had to be held just above the melting point of barium. The emission of a pale green color from the discharge mixture was indicative of the presence of barium vapor.

Successive scans covering 100 MHz in frequency were initially recorded to identify features. The actual frequencies were measured from scans 5 MHz in frequency coverage. As many as 16 averages were found necessary for the weaker features of ^{137}BaNH and ^{137}BaND.

Computational Methods. Electronic structure calculations were carried out to compare experimental and calculated geometries and vibrational frequencies and to examine the electron distribution and bonding in the ground state of BaNH and related molecules. Calculations were performed using the package ADF 2004.01, which has been widely utilized for studies of molecules containing heavy elements.[19] The method uses extensive Slater-type basis functions and has been developed with an account of scalar relativistic effects by means of the Zero Order Regular Approximation (ZORA[20]). The all-electron relativistic TZ2P basis set as defined in the ADF package was used without freezing of core functions. This basis is Slater triple-ζ quality for the critical valence functions and includes virtual polarization p and d functions on H, virtual d and f functions on N, and virtual 5d, 6p, and 4f functions on Ba. The all-electron expansion of this set (with the number of functions of each type in parentheses) is [Ba: 1s(3)2s(2)2p(3)3s(2)3p(2)3d(2)4s(2)4p(2)4d(3)5s(2)5p(3)6s(3)*5d(2)4f(2)6p(1)*; N: 1s(2)2s(3)2p(3)*3d(1)4f(1)*; H: 1s(3)*2p(1)3d(1)*], where the polarization functions indicated by italics are unoccupied (virtual) for the neutral atoms. The ADF calculations were carried out with the VWN local density approximation[21] and the PW91 exchange-correlation correction (PW91).[22] For comparison, the structures also were optimized with the small core DZ (double-ζ) and TZP (triple-ζ with polarization basis sets and with the Slater Xα functional ($\alpha = {}^2/_3$) without corrections (exchange only), with addition of the VWN local correlation approximation without corrections (VWN), with addition of the Becke−Perdew exchange-correlation corrections (BP86), and with the Slater Xα exchange-only local density approximation and Becke−Lee−Yang−Parr exchange-correlation corrections (BLYP). References to these other basis sets and functionals are available in the ADF documentation.[19] The optimized bond distances from these different functionals with the TZ2P basis were the same within ±0.02 Å. The optimized Ba−N distance varied from 2.075 Å (TZ2P relativistic) to 2.158 Å (DZ nonrelativistic) with the VWN/PW91 functional, but the same bonding principles were evident. Only the VWN/PW91 calculations with the TZ2P basis are reported in detail.

Geometry optimization of BaNH was carried out in each case with an integration accuracy of 8.0 and converged to an energy of 0.0001 au and a maximum gradient of 0.0005. Vibrational frequencies were calculated (with the same integration accuracy) by numerical differentiation of the energy gradients with both positive and negative displacements from the equilibrium geometry, and the accuracy (within 1 cm^{-1}) was tested by varying the displacement amplitudes and coordinates.[23] The same accuracy was utilized for calculations on related

(11) Steimle, T. C.; Xin, J.; Marr, A. J.; Beaton, S. *J. Chem. Phys.* **1997**, *106*, 9084.
(12) Simard, B.; Balfour, W. J.; Vasseur, M.; Hackett, P. A. *J. Chem. Phys.* **1990**, *93*, 4481.
(13) Simard, B.; Jakubek, Z.; Niki, H.; Balfour, W. J. *J. Chem. Phys.* **1999**, *111*, 1483.
(14) Jakubek, Z. J.; Simard, B.; Niki, H.; Balfour, W. J. *J. Chem. Phys.* **2000**, *113*, 3591.
(15) Merer, A. J.; Rixon, S. J.; Varberg, T. D.; Clouthier, D. J. *International Symposium on Molecular Spectroscopy* **2001**, Talk FC06
(16) Gagliardi, L. *J. Am. Chem. Soc.* **2002**, *124*, 8757.
(17) Ziurys, L. M.; Barclay, W. L., Jr.; Anderson, M. A.; Fletcher, D. A.; Lamb, J. W. *Rev. Sci. Instrum.* **1994**, *65*, 1517.
(18) Anderson, M. A.; Allen, M. D.; Barclay, W. L., Jr.; Ziurys, L. M. *Chem. Phys. Lett.* **1993**, *205*, 415.
(19) ADF2004.01, SCM, Theoretical Chemistry, Vrije Universiteit, Amsterdam, The Netherlands (http://www.scm.com). (a) te Velde, G.; Bickelhaupt, F. M.; van Gisbergen, S. J. A.; Fonseca Guerra, C.; Baerends, E. J.; Snijders, J. G.; Ziegler, T. *J. Comput. Chem.* **2001**, *22*, 931. (b) Fonseca Guerra, C.; Snijders, J. G.; te Velde, G.; Baerends, E. J. *Theor. Chem. Acc.* **1998**, *99*, 391.
(20) (a) van Lenthe, E.; Baerends, E. J.; Snijders, J. G. *J. Chem. Phys.* **1993**, *99*, 4597. (b) van Lenthe, E.; Baerends, E. J.; Snijders, J. G. *J. Chem. Phys.* **1994**, *101*, 9783. (c) van Lenthe, E.; Ehlers, A.; Baerends, E. J. *J. Chem. Phys.* **1999**, *110*, 8943.
(21) Vosko, S. H.; Wilk, L.; Nusair, M. *Can. J. Phys.* **1980**, *58*, 1200.
(22) Perdew, J. P.; Chevary, J. A.; Vosko, S. H.; Jackson, K. A.; Pederson, M. R.; Singh, D. J.; Fiolhais, C. *Phys. Rev. B* **1992** *46*, 6671.
(23) (a) Fan, L.; Ziegler, T. *J. Chem. Phys.* **1992**, *96*, 9005. (b) Fan, L.; Ziegler, T. *J. Phys. Chem.* **1992**, *96*, 6937.

molecules and explorations of local minima and transition states on the potential energy surfaces of the reactions discussed later. The entropy and internal energy contributions to the free energy were calculated from 250 K to 1500 K and found to have little influence on the relative energies of the reactants, intermediates, transition states, and products.

Natural bond orbital (NBO[24]) and natural population (NPA[25]) analyses of the BaNH wave function were carried out with the program NBO 5.0.[26] Molecular orbital analysis of the wave function was carried out by expressing the results of the density functional calculation in terms of the Hartree−Fock−Roothaan formalism FC = SCE, where the elements of the Kohn−Sham (Fock) matrix F were obtained by the method of Senthilkumar[27] and transformed to a basis of the Ba atom fragment and NH fragment orbitals. In addition to NPA and Mulliken population analyses, atomic charges also were estimated by the method of Bader's Atoms in Molecules (AIM[28]) with the XAIM program[29] and the methods of Hirshfeld,[30,31] Voronoi Deformation Density (VDD[32]), and multipole derived (MDC-q) as defined in the ADF documentation. The calculated charges of the Ba atom are as follows: NPA, +1.59; AIM, +1.20; Mulliken, +0.73; Hirshfeld, +0.61; VDD, +0.68; MDC-q, +0.71. The orbital plots were generated using the program Molekel.[33] In the figures the outer orbital surface value is ±0.02 and the inner surface value is ±0.05.

Results

Because magnesium, calcium, and strontium all produced amide radicals with $\tilde{X}^2A_1$ ground states on reaction with NH_3, the same product was expected for barium, namely $BaNH_2$.[6−8] The ground state of this molecule is $^2A_1$, and thus an asymmetric top spectrum with a spin-rotation splitting near 70 MHz[18] should have been observed. However, no asymmetric top pattern consisting of doublets was detectable in the data. Instead, a few lines were recorded that appeared to arise from a linear molecule. BaNH was an obvious choice. A range of rotational constants (7919−8208 MHz) was predicted for BaNH based on the Ba−N bond length from calculations of the BaNCs molecule.[16] Then 44 GHz in frequency space were scanned, searching for harmonically related features.

Because the spectrum was contaminated with multiple BaO and BaOH lines, they needed to be eliminated from the search. Fortunately such lines could be identified based on previously published microwave data.[18,34] To further eliminate contaminating features, the original frequency region was rescanned using barium and N_2O as precursors. After identifying the additional contaminants, harmonic relationships among the remaining lines were found. First, rotational transitions originating in the (000) ground vibrational state were identified, followed by those of the (010) bending and (100) heavy atom stretching vibrations. Some additional scanning was needed to locate these latter features. A similar procedure was conducted to obtain the spectrum of BaND, based on estimated rotational constants. Finally, the rotational constants for the less abundant ^{137}BaNH and ^{137}BaND isotopomers were predicted, based on an r_0 structure established from the barium-138 data, and their spectra were readily located. (The ^{138}Ba:^{137}Ba ratio is 71.7:11.2.)

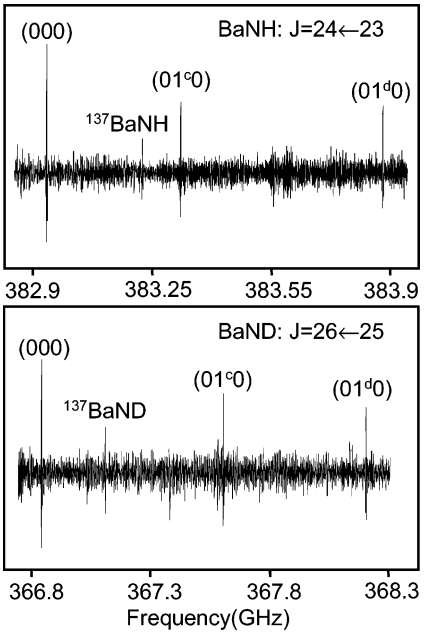

Figure 1. Representative spectra of BaNH and BaND in their $X^1\Sigma^+$ ground electronic states.

Figure 1 displays representative spectra of BaNH and BaND. In the top panel, the $J = 24 \leftarrow 23$ transition of BaNH is displayed. The rotational pattern coincides with that of a linear molecule. Features arising from the ground state and the (010) bending mode, split by 565 MHz due to the l-type doubling, are visible in the spectra. The ^{137}BaNH ground-state line is positioned between the (000) mode and the lower component of the (010) mode of the barium-138 isotopomer. Not visible in the figure is the heavy atom stretch (100), located 1440 MHz to the lower frequency with respect to the (000) line.

The BaND spectrum, shown in the lower panel, resembles that of BaNH. Here the (000) line and the l-type doublets of the bending mode of the $J = 26 \leftarrow 25$ transition are displayed. Again, the same transition of the less abundant ^{137}BaND isotopomer is located between the (000) and the (01^{c}0) lines.

Twelve transitions each were measured for the (000), (010), and (100) vibrational modes of ^{138}BaNH and ^{138}BaND. For the barium-137 species, 12 rotational transitions were recorded, only for the ground vibrational state. The transition frequencies are listed in Table 1.

Analysis

The data for BaNH were analyzed with a $^1\Sigma$ Hamiltonian consisting of molecular frame rotation and the l-type doubling terms:[35]

$$H = H_{\text{rot}} + H_{\text{l-type doubl}} \quad (1)$$

(24) Foster, J. P.; Weinhold, F. *J. Am. Chem. Soc.* **1980**, *102*, 7211.
(25) (a) Reed, A. E.; Weinhold, F. *J. Chem. Phys.* **1983**, *78*, 4066. (b) Reed, A. E.; Weinstock, R. B.; Weinhold, F. *J. Chem. Phys.* **1985**, *83*, 735.
(26) NBO 5.0. Glendening, E. D.; Badenhoop, J, K.; Reed, A. E.; Carpenter, J. E.; Bohmann, J. A.; Morales, C. M.; Weinhold, F. Theoretical Chemistry Institute, University of Wisconsin, Madison, 2001.
(27) (a) Senthilkumar, K.; Grozema, F. C.; Bickelhaupt, F. M.; Siebbeles, L. D. A. *J. Chem. Phys.* **2003**, *119*, 9809. (b) Senthilkumar, K.; Grozema, F. C.; Fonseca Guerra, C.; Bickelhaupt, F. M.; Siebbeles, L. D. A. *J. Am. Chem. Soc.* **2003**, *125*, 13658.
(28) Bader, R. F. W. *Atoms in Molecules. A Quantum Theory*; Clarendon Press: Oxford, U.K., 1990.
(29) Xavi López, Engelber Sans, and Carles Bo, Departament de Química Física i Inorgànica Universitat Rovira i Virgili, Tarragona, Spain, http://www.quimica.urv.es/XAIM/.
(30) Hirshfeld, F. L. *Theor. Chim. Acta* **1977**, *44*, 129.
(31) Parr, R. G.; Ayers, P. W.; Nalewajski, R. F. *J. Phys. Chem. A* **2005**, *109*, 3957.
(32) Guerra, C. F.; Handgraaf, J.-W.; Baerends, E. J.; Bickelhaupt, F. M. *J. Comput. Chem.* **2003**, *25*, 189.
(33) MOLEKEL 4.3. Flükiger, P.; Lüthi, H. P.; Portmann, S.; Weber, J. Swiss Center for Scientific Computing, Manno (Switzerland), 2000−2002. Portmann, S.; Lüthi, H. P. *CHIMIA* **2000**, *54*, 766.
(34) Hocking, W. H.; Pearson, E. F.; Creswell, R. A.; Winnewisser, G. *J. Chem. Phys.* **1978**, *68*, 1128.

Table 1. Observed Rotational Transitions of BaNH ($X^1\Sigma^+$)[a]

			^{138}BaNH		^{137}BaNH		^{138}BaND		^{137}BaND	
$(\nu_1\nu_2\nu_3)$	$J \leftarrow J'$		ν_{obsd}	$\nu_{obsd} - \nu_{calcd}$	ν_{obsd}	$\nu_{obsd} - \nu_{calcd}$	ν_{obsd}	$\nu_{obsd} - \nu_{calcd}$	ν_{obsd}	$\nu_{obsd} - \nu_{calcd}$
(000)	19−18		303 254.727	0.019	303 468.349	0.008				
	20−19		319 197.521	0.023	319 422.390	0.039				
	21−20		335 137.526	0.005	335 373.557	−0.034				
	22−21		351 074.639	0.000	351 321.930	0.008				
	23−22		367 008.699	−0.014	367 267.187	−0.018	324 575.148	0.038	324 815.059	0.030
	24−23		382 939.601	−0.004	383 209.275	−0.028	338 668.050	0.023	338 918.366	0.015
	25−24		398 867.167	−0.011	399 148.099	0.023	352 758.509	−0.005	353 019.275	0.037
	26−25		414 791.272	−0.019	415 083.393	0.007	366 846.457	−0.011	367 117.565	−0.024
	27−26						380 931.777	−0.011	381 213.305	0.002
	28−27						395 014.363	−0.010	395 306.270	−0.007
	29−28		462 541.490	−0.008	462 867.153	0.000	409 094.116	−0.006	409 396.358	−0.054
	30−29		478 450.372	−0.022	478 787.190	−0.036				
	31−30		494 355.152	0.013	494 703.176	0.033				
	32−31		510 255.620	0.023	510 614.764	−0.002	451 315.348	0.010	451 648.713	−0.045
	33−32						465 382.722	−0.007	465 726.524	0.007
	34−33						479 446.682	−0.095	479 800.928	0.000
	35−34						493 507.389	0.008	493 871.934	0.045
	36−35						507 564.514	0.074	507 939.127[b]	
(01^10)										
	19−18	c	303 555.077	0.065						
	19−18	d	304 002.658	0.031						
	20−19	c	319 513.200	0.012						
	20−19	d	319 984.246	0.025						
	21−20	c	335 468.518	−0.015						
	21−20	d	335 962.981	0.020						
	22−21	c	351 420.902	−0.003						
	22−21	d	351 938.725	0.019						
	23−22	c	367 370.204	0.042			325 255.987	−0.001		
	23−22	d	367 911.291	−0.022			325 795.570	0.045		
	24−23	c	383 316.090	−0.073			339 378.060	0.029		
	24−23	d	383 880.610	−0.028			339 940.832	0.033		
	25−24	c	399 258.734	−0.033			353 497.567	−0.014		
	25−24	d	399 846.512	−0.029			354 083.567	0.014		
	26−25	c	415 197.827	−0.004			367 614.517	−0.019		
	26−25	d	415 808.841	−0.035			368 223.677	−0.003		
	27−26	c					381 728.789	−0.001		
	27−26	d					382 361.046	−0.030		
	28−27	c					395 840.271	0.030		
	28−27	d					396 495.589	−0.047		
	29−28	c	462 992.345	−0.029			409 948.735	−0.050		
	29−28	d	463 673.068	0.009			410 627.219	−0.036		
	30−29	c	478 915.882	0.016						
	30−29	d	479 619.685	−0.019						
	31−30	c	494 835.123	0.011						
	31−30	d	495 562.070	0.002						
	32−31	c	510 749.989	0.021			452 255.919	−0.012		
	32−31	d	511 500.046	0.035			453 003.422	0.008		
	33−32	c					466 351.819	0.013		
	33−32	d					467 122.210	−0.007		
	34−33	c					480 444.296	0.042		
	34−33	d					481 237.564	0.010		
	35−34	c					494 533.215	0.043		
	35−34	d					495 349.319	−0.001		
	36−35	c					508 618.394	−0.061		
	36−35	d					509 457.429	0.021		
(100)										
	19−18		302 115.604	0.036						
	20−19		317 998.314	0.038						
	21−20		333 878.210	0.012						
	22−21		349 755.201	0.007						
	23−22		365 629.112	−0.014			324 268.523	0.025		
	24−23		381 499.777	−0.076			338 344.511	0.002		
	25−24		397 367.215	−0.022			352 417.669	0.020		
	26−25		413 231.168	0.031			366 487.783	−0.020		
	27−26						380 554.810	−0.045		
	28−27						394 618.682	−0.007		
	29−28		460 800.507	−0.042			408 679.181	−0.009		
	30−29		476 649.099	−0.026						
	31−30		492 493.561	0.039						
	32−31		508 333.625	0.026			450 839.567	0.005		
	33−32						464 885.675	0.078		
	34−33						478 927.718	−0.016		
	35−34						492 965.829	−0.032		
	36−35						506 999.868	0.001		

[a] In MHz. [b] Blended line; not fit.

Table 2. Rotational Constants for ^{138}BaNH, ^{137}BaNH, ^{138}BaND, ^{137}BaND ($X^1\Sigma^+$)[a]

$(\nu_1\nu_2\nu_3)$		^{138}BaNH	^{137}BaNH	^{138}BaND	^{137}BaND
(000)	B	7984.5488(29)	7990.1761(29)	7060.4461(28)	7065.6682(31)
	D	0.005 764 2(19)	0.005 771 7(19)	0.004 220 7(14)	0.004 226 7(17)
(01^10)	B	7998.4427(21)		7081.2423(20)	
	D	0.005 921 2(14)		0.004 351 8(10)	
	q_v	−11.8120(41)		−11.7821(40)	
	q_D	4.52×10^{-5}(27)		5.01×10^{-5}(20)	
(100)	B	7954.6008(29)		7054.641(13)	
	D	0.005 804 8(19)		0.005 053(14)	
	H_v			2.40×10^{-8}(51)	
rms deviation		0.029	0.024	0.032	0.030

[a] In MHz; errors are 3σ.

The data sets for each isotopomer were analyzed separately. For a given isotopomer, the different vibrational states were fit individually. An rms of the fit for each isotopomer was generated by considering the residuals of all vibrational states for that particular species. The resulting spectroscopic parameters for the four isotopomers are listed in Table 2. The ground vibrational and (100) states needed only B and D constants in the analysis, while the (010) satellite lines also required the l-type doubling constant q, and its centrifugal distortion correction, q_D. To fit the transitions for the ^{138}BaND species, H_v, the sixth-order distortion constant was needed as well. The corresponding rms for all isotopomers lies between 24 and 32 kHz.

Based on the rotational constants for all four isotopomers, r_0, $r_m^{(1)}$, and r_S structures were calculated. The r_0 and $r_m^{(1)}$ structures were determined by a nonlinear least-squares fit to the four moments of inertia using the STRFIT program.[37] The r_0 structure for the molecule yielded $r_{Ba-N} = 2.078$ Å and $r_{N-H} = 1.011$ Å. The standard deviations on these numbers are ±0.000 001 Å but do not reflect their true uncertainty, which arises from zero-point vibration and is typically ±0.001 Å.

An r_S structure of $r_{Ba-N} = 2.076 \pm 0.0003$ Å and $r_{N-H} = 1.013 \pm 0.0003$ Å was determined, based on Kraitchman's equations.[38] (The uncertainties here were derived by propagating those established for the rotational constants.) The four isotopomers were also used to determine an $r_m^{(1)}$ structure,[39] which is $r_{Ba-N} = 2.077 \pm 0.002$ Å and $r_{N-H} = 1.0116 \pm 0.0006$ Å with a correction factor in the b direction being $b_{corr} = 0.004\,291\sqrt{\text{amu}}$ Å. This correction factor modifies the moment of inertia tensor to account for some of the zero-point vibrations, as modeled by Watson et al. (ref 39). As a consequence, the $r_m^{(1)}$ structure is thought to be superior to the r_S and r_0 geometries. However, the small difference between the r_0 and $r_m^{(1)}$ structures shows that the effect of the zero-point vibration on the geometry is small. The molecule is considered therefore to be fairly rigid.

Estimates of the vibrational frequencies were calculated for BaNH as well. The Kratzer equation was used to compute the heavy atom stretch,[40] assuming the N−H group to be a single moiety:

$$\omega_1 = \sqrt{\frac{4B_0^3}{D_0}} \tag{2}$$

For the heavy atom stretch of BaNH, this estimate results in $\omega_1 = 627$ cm^{-1}, while, for the deuterated species, $\omega_1 = 609$ cm^{-1}.

The bending mode vibration can be derived from the l-type doubling constant q via the relationship:[36]

$$q \approx \frac{2.6\, B_e^2}{\omega_2} \tag{3}$$

Since rotational transitions of the NH stretching mode, (001), were not measured, B_e must be replaced by $\tilde{B}_e$, where $B_v = \tilde{B}_e - \alpha_1(v + {}^1/_2) - \alpha_2(v + 1)$. Substituting the experimental $B_{v=0}$ for the stretching and bending modes results in $\tilde{B}_e = 7985.6289$ MHz for BaNH and $\tilde{B}_e = 7042.5525$ MHz for BaND, which results in ω_2 values of 468 and 365 cm^{-1}, respectively. The uncertainties of these vibrational frequencies range from 1 to 2% for ω_1 and are roughly 15% for ω_2.

DFT Calculations on BaNH

The density functional calculations agree with the linear structure of BaNH and yield calculated values for the bond distances and vibrational frequencies that are in excellent agreement with those determined from analysis of the rotational spectra above, as shown in Table 3. The optimized Ba−N bond distance obtained by the PW91/TZ2P calculation of 2.075 Å is essentially the same as the experimental r_0(Ba−N) distance of 2.078 Å, and the optimized N−H distance of 1.027 Å compares well with the experimental r_0(N−H) distance of 1.011 Å. The calculated and experimental vibrational frequencies also agree to better than 15% (see Table 3). According to the potential surface given by the calculations, the ground ω_2 bending vibrational state sweeps out a Ba−N−H angle of about 17° from the linear structure, in agreement with the fairly rigid structure indicated by experiment. The agreement between these experimental and computational results indicates, on one hand, that the interpretation and the analysis of the spectral data are valid and, on the other hand, that the theoretical electron density

(35) Thorwirth, S.; Müller, H. S. P.; Lewen, F.; Gendriesch, R.; Winnewisser, G. *Astron. Astrophys.* **2000**, *L37*, 363.
(36) Townes, C. H.; Schawlow A. L. *Microwave Spectroscopy*; Dover Publications: 1975.
(37) Kisiel, Z. *J. Mol. Spectrosc.* **2003**, *218*, 58.
(38) Gordy, W.; Cook, R. L. *Microwave Molecular Spectra*; John Wiley & Sons: 1984.
(39) Watson, J. K. G.; Roytburg, A.; Ulrich, W. *J. Mol. Spectrosc.* **1999**, *196*, 102.
(40) Kratzer, A. *Z. Phys.* (Leipzig), **1920**, *3*, 289.

Table 3. Bond Lengths and Vibrational Frequencies of BaNH ($X^1\Sigma^+$)[a]

	experimental		theoretical	
	r_{Ba-N} (Å)	r_{N-H} (Å)	r_{Ba-N} (Å)	r_{N-H} (Å)
r_0	2.078(3)	1.011(3)		
r_S	2.076(1)	1.013(1)		
$r_m^{(1)}$[b]	2.077(6)	1.012(2)		
r_e			2.075	1.027

frequency (cm^{-1})	BaNH	BaND	BaNH	BaND
ω_1	627	609	635	616
ω_2	468	365	426	321
ω_3			3369	2467

[a] Errors are 3σ. [b] For $b_{corr} = 0.004291\sqrt{\text{amu}}$ Å.

obtained from these calculations gives good account of the bonding in BaNH in the potential energy region near the equilibrium structure. The electron distribution and bonding in BaNH according to this wave function will be analyzed in detail in the discussion section that follows.

As mentioned in the Experimental Section, a variety of local density approximations and generalized gradient corrections give the same structures with the same bond distances within ±0.02 Å. Although the best agreement with experiment is obtained with the TZ2P basis and the scalar relativistic effects, the dependence on different standard basis sets and relativistic effects also is not dramatic, and even the DZ basis gives reasonable results. However, it should be noted that the DZ basis has 5d, 6p, and 4f polarization functions on the Ba atom. In anticipation of the discussion of the bonding in BaNH, it is noted that removal of the virtual 5d functions from the basis has dramatic effects on the calculated bond distances. In the case of the DZ basis, removal of the Ba 5d function results in a 0.35 Å increase in the optimized Ba−N distance, a change comparable to the increase in C−C distance from triple-bonded acetylene to single-bonded ethane. The role of the virtual Ba 5d functions in charge delocalization and bonding with the imide fragment is an important aspect of the bonding analysis in the next section.

Discussion

When magnesium, calcium, and strontium are reacted with ammonia, they produce metal amide radicals of the form MNH_2 with C_{2v} symmetry. In contrast, the present results show that the same reaction with barium yields BaNH, a linear imide species. The IIIB transition metals Sc, Y, and La produce imides as well. Buckner has proposed a mechanism for M^+ cations reacting with ammonia to form MNH^+ molecules as shown in Figure 2.[41] The mechanism involves initial coordination of NH_3 to the metal center followed by the oxidative addition of an N−H bond to the metal. The intermediate hydrido-amido-metal complex in the proposed mechanism leads to the radical metal amide via a homolytic hydrogen−metal bond dissociation (route 1). In the case of V^+ and higher d-electron count transition metals, the intermediate hydrido-amido-metal complex may undergo an α hydrogen migration onto the metal center, followed by reductive elimination of H_2 (route 2) to yield the metal-imide species. This route seems unlikely for barium, as the H_2 elimination by route 2 proceeds through an intermediate

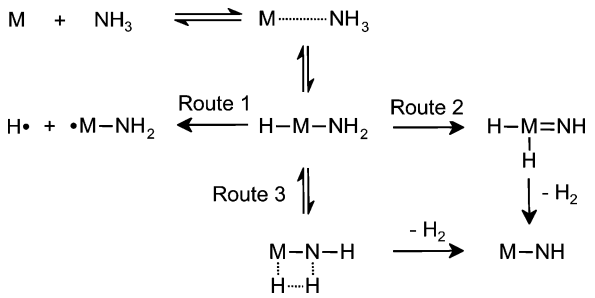

Figure 2. Mechanism for the metal−ammonia reaction proposed by Buckner et al. for a variety of metals.[41]

with Ba in a formal +4 oxidation state. Alternatively, the hydrido-amido-metal complex can eliminate H_2 via a four-center intermediate (route 3).

Further study is needed to clarify the mechanism and the factors that favor imido formation, but the availability of appropriate electron acceptor orbitals on the metal atom is an important aspect. The role of acceptor orbitals on the metal has been implicated in several theoretical studies by different techniques on related molecules. Siegbahn and co-workers have investigated the oxidative addition of N−H bonds to second-row transition metal atoms with geometries optimized at the self-consistent-field Hartree−Fock level and with relative energies estimated by the modified coupled pair functional (MCPF) method.[42] These authors point out that transition metals on the left side of the second row favor the interaction with ammonia and formation of planar hydrido-amido-metal oxidative addition products because the empty 4d orbitals on the metal allow π donation from the nitrogen lone pair. Transition metals to the right of the row do not have the available empty d orbitals and leave the extra nitrogen electrons localized on the nitrogen in lone pairs, and the nitrogen atom reverts to a pyramidal structure. Gagliardi reported a series of density functional and higher level calculations with extensive Gaussian basis sets on MNM′ triatomic molecules, where M is an alkaline earth metal (Ca, Sr, Ba) and M′ is an alkali metal (K, Rb, Cs).[16] Based on these calculations, she proposed that the Ba−N bond in the BaNK and BaNCs compounds has one σ and two π bonds. The presence of multiple bonds results in cylindrical symmetry in the system and a linear structure. Balasubramanian reported multireference CI/CASSCF calculations, again with Gaussian basis sets, on YNH.[43] The structure is linear, and most of the π bonding between Y and N is due to Y(dπ)−N(pπ) interaction.

Structural comparisons also indicate the effects of multiple Ba−N bonding. The Ba−N bond length of 2.078 Å in BaNH found here is much shorter than the Ca−N bond length of 2.126 Å in $CaNH_2$ and the Sr−N bond length of 2.256 Å in $SrNH_2$.[7,8] Because barium is a larger atom than calcium and strontium the decrease in bond distance is indicative of increased bond order between the barium and nitrogen atoms.

The density functional electronic structure calculations reported here give excellent agreement with the experimental geometry and vibrational frequencies of BaNH, indicating that the calculated wave function is a good representation of the bonding in the ground state of this molecule in the region of the equilibrium structure. The natural bond orbital analysis of

(41) Buckner, S. W.; Gord, J. R.; Freiser, B. S. *J. Am. Chem. Soc.* **1988**, *110*, 6606.
(42) Blomberg, M. R. A.; Siegbahn, P. E. M.; Svensson, M. *Inorg. Chem.* **1993**, *32*, 4218.
(43) Das, K. K.; Balasubramanian, K. *J. Chem. Phys.* **1990**, *93*, 6671.

Table 4. Natural Bond Orbital Analysis of BaNH[a]

Natural Orbitals[b]		
NBO type	occupancy	hybrid composition[c,d]
N−H σ bond	1.99	70% N $sp^{0.73}$ + 30% H s
Ba−N σ bond	1.95	93% N $sp^{1.38}$ + 7% Ba $p^{0.18}df^{0.08}$
Ba−N π bonds	4.00	91% N p + 9% Ba d

Natural Population Analysis		
	charge	electron configuration
Ba	+1.59	[core]6s(0.01)4f(0.02)5d(0.48)-6p(0.01)6d(0.01)
N	−1.91	[core]2s(1.77)2p(5.14)
H	+0.32	1s(0.67)

[a] The natural Lewis structure represents 99.7% of the total electron density. [b] Natural Bond Orders: Ba−N, 2.95; N−H, 0.95. [c] Hybrid contributions listed if greater than 0.03. [d] Ba hybrids are formed from the 5p, 5d, and 4f functions.

Table 5. Valence Molecular Orbitals of BaNH[a]

		orbital characters[c]			overlap populations		
orbital[b]	energy	Ba	N	H	Ba–N	N–H	Ba–NH
$1\pi_x,1\pi_y$	−3.02 eV	22% 5d	74% 2p	2% 2p	0.353	0.072	0.364
3σ	−5.52 eV	4% 6s	11% 2s	20% 1s			
		6% 5p	40% 2p		0.078	−0.174	−0.070
		17% 5d					
2σ	−13.92 eV	34% 5p	32% 2s	25% 1s	−0.270	0.569	−0.372
			7% 2p	2% 2p			
1σ	−17.36 eV		35% 2s	7% 1s	0.290	0.171	0.315
		57% 5p	1% 2p	1% 2p			
total populations		5pσ 1.95	2s 1.60	1s 1.04	0.858	0.709	0.653
		5dσ 0.36	2pσ 0.97	2pσ 0.05			
		5dπ 0.90	2pπ 2.98	2pπ 0.09			

[a] See Experimental Section for details of computational model and population analysis. Characters and population analyses are Mulliken [b] Omitted from the table are the inner valence Ba 5pπ (>99%) orbitals at −15.93 eV. [c] See Figure 3 for orbital plots.

the electronic structure of BaNH is summarized in Table 4. According to this analysis, the leading Lewis structure of the bonding is represented as Ba≡N−H with a resonance weight of 95%. The N−H σ bond is formed primarily from a nitrogen sp hybrid orbital and the H 1s orbital, and the Ba−N σ bond is formed primarily from the other nitrogen sp hybrid orbital and the barium 5dσ orbital. The two Ba−N π bonds are formed from the nitrogen 2pπ orbitals and the barium 5dπ orbitals. As a result the Ba−N natural bond order is 2.95 and the N−H natural bond order is 0.95. The total Ba−N bond order is 84% ionic according to the natural orbital analysis. The natural orbital description of the bonding is then the same as the traditional view of a ligand bonding to a transition metal, in which formal oxidation states are determined by counting the electrons for closed-shell ligands, and the metal−ligand σ bond is formed from donation of a ligand electron pair to an empty metal d orbital to form a dative σ bond. If the ligand has filled π orbitals and the metal has empty dπ orbitals, the ligand can donate π electron density to the metal. In this case the formal NH^{-2} ligand forms a σ bond to the formal Ba^{2+} metal by donating electrons from the filled nitrogen sp σ lone pair orbital to the empty Ba 5dσ orbital, and the filled nitrogen 2pπ orbitals form π bonds by donating to the empty Ba 5dπ orbitals. According to the conventions of natural bond orbital analysis, the resulting orbitals are considered bonds if at least 5% of the population is on the barium center, as found in this case.

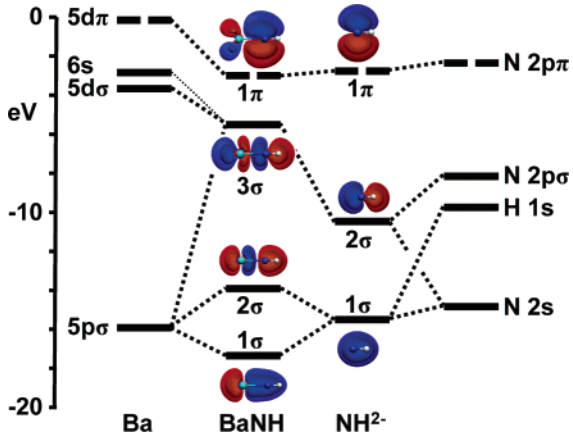

Figure 3. Molecular orbital energy level diagram of BaNH. The Ba, N, H, and NH^{-2} fragment energies are the diagonal Kohn−Sham Fock energies of these basis functions in the density distribution of the BaNH molecule. The outer orbital surface value is ±0.02.

The natural bond orbital analysis is in terms of the natural atomic orbitals, which contain nodal features in their outer tails to ensure interatomic orthogonality. As a consequence, for BaNH with the large core on barium, the natural population analysis overemphasizes the negative charge on nitrogen and underemphasizes the charge donation to barium.[32] For comparison, Table 5 summarizes the characters of the valence canonical delocalized molecular orbitals in terms of the one-center atomic orbitals. Here it is seen that the π bond is 22% barium in character, and the σ bonds are delocalized across the three atoms of the molecule. A surface plot of the π bond is shown below with an outer shell surface value of ±0.02 and an inner surface value of ±0.05. The plot shows the overlap and occupation of the d orbital of the Ba atom on the left with the filled N p orbital of the N−H group on the right.

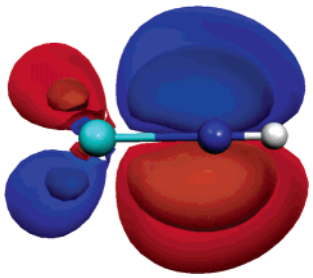

The basis for these interactions is clear from the molecular orbital diagram in Figure 3. The Ba 5dπ orbitals are only slightly less stable than the N 2pπ orbitals in the charge distribution of BaNH and are in a favorable energy position for bond formation. The Ba 6s orbital is less stable than the Ba 5dσ in the charge distribution of the molecule and contributes little to the σ bond formation. This point will become important later. The nitrogen pσ lone pair donates to the Ba $5dz^2$ orbital in the 3σ molecular orbital. The total Ba−N overlap population is comparable to the N−H overlap population, but with most of the overlap population coming from the Ba−N π bonds.

Table 5 also shows the redistribution of charge resulting from the σ and π bond formation between the formal Ba^{2+} and NH^{-2} ions. More than a full electron of charge is donated from NH^{-2} to Ba^{2+}. The charge on the Ba atom is substantially reduced from +2 (as evaluated by a number of different methods of

Table 6. Selected Structure and Bonding Properties Calculated for MNH_2 and MNH[a,b]

	Mg	Ca	Sr	Ba
		MNH_2		
r_e(M−N)	1.91 (1.90)	2.10 (2.13)	2.24 (2.26)	2.34
r_e(N−H)	1.02 (1.01)	1.02 (1.02)	1.02 (1.02)	1.02
M−N−H angle	126° (126°)	127° (127°)	128° (127°)	127°
M−N π bond character	85% N 2p 8% Mg 3p	82% N 2p 8% Ca 3d	84% N 2p 8% Sr 4d	83% N 2p 10% Ba 5d
M ns e^- pop.[c]	0.99	0.93	0.95	0.87
ϵ(M−N π bond)[d]	−4.85	−4.77	−4.45	−4.67
ϵ(SOMO)[d]	−4.39 (Mg 3s)	−3.29 (Ca 4s)	−3.14 (Sr 5s)	−2.78 (Ba 6s)
ΔE to MNH	6.13	5.50	5.57	4.77
		MNH		
r_e(M−N)	1.86	1.90	2.03	2.08 (2.08)
r_e(N−H)	1.04	1.03	1.03	1.03 (1.01)
M−N−H angle	110°	158°	151°	180° (180°)
M−N "bent π" bond character[e]	53% N 2p 32% Mg 3s	72% N 2p 14%Ca 3d 5% Ca 4s	72% N 2p 13% Sr 4d 7% Sr 5s	74% N 2p 22% Ba 5d
M ns e^- pop.[c]	0.87	0.23	0.30	0.05

[a] Distances in Å, energies in eV. [b] Experimental values in parentheses are taken from ref 3. [c] Electron populations in the Mg 3s, Ca 4s, Sr 5s, and Ba 6s orbitals. [d] Kohn−Sham orbital energies. The SOMO is the singly occupied, predominantly M valence s orbital. [e] Orbital in the bent MNH molecular plane that correlates with a M−N π bond in linear MNH.

charge analysis, see Experimental Section) indicating a substantial difference from a purely ionic model for the description of the bonding in this molecule.

The significance of the π bonding is demonstrated also by comparing BaNH with BaOH and LaNH. The heavy atom stretching frequency for BaOH is 492 cm^{-1} and for BaNH is 627 cm^{-1}.[44] After accounting for the difference in mass, these frequencies indicate that the Ba−N bond is stronger. Similarly, the Ba−O bond length in BaOH (2.20 Å) is longer than the Ba−N bond length in BaNH (2.08 Å), which is opposite to the relative sizes of the oxygen and nitrogen atoms. The changes occur because BaOH has one more valence electron than BaNH. A similar calculation for BaOH to that of BaNH (except with an unrestricted open shell) agrees with the linear structure and matches the experimental interatomic distances well (Ba−O 2.19 Å calcd compared to 2.20 Å expt; O−H 0.96 calcd compared to 0.92 Å expt). The extra electron in the BaOH molecule is in a nonbonding orbital on Ba (86% 6s, 7% 6pσ, 5% 5dσ), and the formal bond orders do not change. Because the extra electron is in a σ orbital the structure stays linear. There are still π Ba−O bonds, but because the O orbitals are more stable due to the additional nuclear charge of oxygen and the Ba orbitals are less stable due to the extra electron charge on Ba, the π bonds are less delocalized from the O 2pπ orbitals to the Ba 5dπ orbitals (10% Ba for BaOH compared to 22% Ba for BaNH). The decreased π bond strength lowers the stretching frequencies and lengthens the Ba−O distance compared to Ba−N. For BaO, a molecule isoelectronic with BaNH, the increased negative charge on the oxygen atom increases the O 2pπ delocalized bonding to the Ba 5dπ orbitals to 16%, and the BaO bond distance shortens (calcd 1.96 Å; expt 1.94 Å).[45]

The LaNH molecule also has been investigated in the gas phase. The heavy atom stretch vibration was measured at $\omega_1 =$ 752 cm^{-1}, and the bending vibration, at $\omega_2 = 464$ cm^{-1}.[15] These frequencies are close to those of BaNH, suggesting similar bonding in these molecules. Like BaOH, LaNH also has one more valence electron than BaNH, and it resides in a similar nonbonding primarily 6s orbital on La. However, in this case the effect of the extra electron charge on the metal is compensated by the extra nuclear charge of the metal, and the relative energies of the 5dπ orbitals are little affected. A calculation on the LaNH molecule gives the same 22% delocalization of the π bond to the heavy metal atom as found in the BaNH calculation and supports the similar bonding in these two molecules. The π bonding obviously contributes to the structure and rigidity of molecules other than BaNH, and the extent of this bonding is dependent on the relative energies of the orbitals.

The question remains as to why the reactions of ammonia with Mg, Ca, and Sr produce MNH_2 metal-amido species and the reaction of ammonia with Ba favors the MNH metal-imido species. Table 6 collects some selected structure and bonding features calculated for the MNH_2 and MNH molecules. There is surprisingly little difference in the calculated properties of the three known $MgNH_2$, $CaNH_2$, and $SrNH_2$ molecules and the hypothetical $BaNH_2$ molecule. The calculations do a good job of reproducing the internuclear distances and bond angles of the known MNH_2 molecules where M is Mg, Ca, and Sr.[6] The only significant difference between the calculated electronic structures of these molecules is that the predominantly metal ns orbital becomes successively less stable with metal substitution down the group. This turns out to have substantial consequences for the structures and formation of the MNH metal-imide species.

A direct consequence of the decreasing stability of the ns orbital down the group is a decreasing energy required to remove a hydrogen atom from MNH_2 to form MNH, as shown in Table 6. This is because removal of a hydrogen atom from MNH_2 is accompanied by a change in electron configuration in which the one electron in the nonbonding metal ns SOMO is transferred to the more stable nitrogen orbital that was bonding with the hydrogen. Because this metal ns orbital is least stable in the case of Ba, the BaNH molecule gains more stabilization energy with this electron transfer. In other words, removal of the hydrogen atom results in electron transfer from the metal to the imide and oxidation of the metal center, and oxidation

(44) Kinsey-Nielsen, S.; Brazier, C. R.; Bernath, P. F. *J. Chem. Phys.* **1986**, *84*, 698.
(45) Wharton, L.; Klemperer W. *J. Chem. Phys.* **1963**, *38*, 2705.

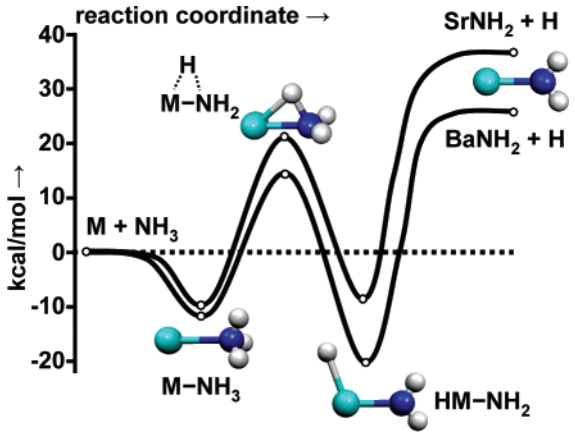

Figure 4. Calculated energies of Ba and Sr reactions with ammonia relative to the energies of the reactants along the indicated reaction coordinate. Optimized structures for the Ba species at the points of the open circles are shown. The structures for Sr species are similar except for the shorter M−N distance due to the smaller Sr atom.

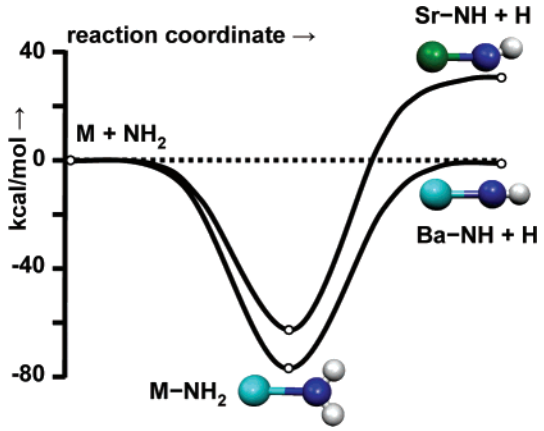

Figure 5. Calculated energies of Ba and Sr atoms interacting with the amidogen radical (NH_2) relative to the energies of the reactants along the indicated reaction coordinate. Optimized structures at the points of the open circles are shown. For the intermediate only the structure for M = Ba is shown. The structure of the intermediate for M = Sr is similar (see Table 6) except for the shorter M−N distance due to the smaller Sr atom.

of the barium atom requires less energy than oxidation of the atoms above it in the group. The calculations indicate that this electron rearrangement from the metal to the nitrogen accounts for about half of the reduction in energy for removal of the H atom from $BaNH_2$ in comparison to the other molecules. The remaining reduction in energy comes from the rearrangement in geometry of the MNH molecule in response to the loss of the H atom. A striking difference between the BaNH molecule compared to the MgNH, CaNH, and SrNH molecules is that the BaNH angle rearranges to 180°, while the other molecules remain bent. This also is a consequence of the more stable s orbitals for Mg, Ca, and Sr in comparison to Ba. These molecules bend to donate N 2p electron density back into the metal ns orbitals at the expense of the N 2pπ to metal $(n-1)$dπ bonding. The Mg atom does not substantially use its 3d orbitals in bonding, and therefore the MgNH molecule has the largest calculated bend. Because the Ba ns orbital is less stable there is less gained from bending and donating to that orbital, and the molecule instead optimizes the N 2pπ to Ba 5dπ bonding with the linear structure. The substantial difference in donating to the metal ns orbitals is shown by the populations of these orbitals in the table. These differences between Ba and the lighter metals are likely to play an important role in the relative stability of transition states and intermediates in the reaction mechanism.

Figure 4 shows the calculated relative energies of NH_3 interacting with Ba and Sr atoms along the reaction coordinate leading to the metal-amide species as proposed for other metals (Figure 2).[41] The Sr atom represents the trend to the lighter Ca and Mg atoms, which are not shown for clarity. The initial coordination of NH_3 to these metals is relatively weak, and the M−N distances are fairly long. This might be expected since the valence ns^2 configurations of these metals lead to filled−filled orbital interactions with the NH_3 lone pair. Oxidative addition of an N−H bond to the metal does produce a hydrido-amido-metal intermediate with a planar structure similar to that investigated for second row transition metals.[42] The intermediate is relatively more stable for M = Ba than for M = Sr, primarily because Ba is more easily oxidized than Sr as discussed above (the first ionization energy of Ba is approximately 11 kcal/mol less than that of Sr[46]). However, the transition state to the intermediate presents a substantial energy barrier to oxidative addition. An even greater barrier must be overcome to completely dissociate the H atom from the intermediate and form the metal-amido species on the right. In sum, interaction of these metals with NH_3 is weak, and formation of the M−N bond for these metals does not provide sufficient energy to break the N−H bond and produce the metal-amido species.

The metal-amido species might be produced if the metal atom and ammonia enter the potential energy surface with sufficient internal energy to overcome these barriers. Additional internal energy is provided by the dc discharge. Some of the metal atoms are in excited electronic states as evidenced by the color of the glow discharge. The first excited electronic state of the Ba atom is the ^{3}D at about 26 kcal/mol above the ground state[46] which is just enough to overcome the barrier to the $BaNH_2$ species. The first excited electronic state of the Sr atom is the ^{3}P at about 41 kcal/mol above the ground state,[46] which also is enough to overcome the barrier to the $SrNH_2$ species. However, the internal energy of the metal atoms in excited electronic states does not explain why $BaNH_2$ would proceed on to BaNH, which requires another 75 kcal/mol according to the calculations, while the others do not. Mechanisms along route 3 of Figure 2, involving H−H bond formation in either a parallel or perpendicular orientation to the Ba−N bond in the transition state with subsequent dissociation of H_2, also were examined, but these mechanisms do not change the basic energy requirement for formation of the metal-imido species.

The NH_3 molecule might also have internal energy from electronic excitation in the dc discharge, and this could assist formation of BaNH. Interestingly, the first singlet excited electronic state of ammonia is only quasi-bound with a low barrier to dissociation to $NH_2 + H$.[47] Indeed, there are several studies of the production of amidogen (NH_2) in dc discharges with ammonia. In our experiment the rotational lines of

(46) Moore, C. E. Atomic Energy Levels as Derived from the Analyses of Optical Spectra Nat. Stand. Ref. Data Ser., Nat. Bur. Stand. (NSRDS−NBS 35 Vol. I−III), CODEN: NSRDA, Washington, DC, 1971.

(47) (a) Hutchison, J. M.; Holiday, R. J.; Bach, A.; Hsieh, S.; Crim, F. F. *J. Phys. Chem. A* **2004**, *108*, 8115. (b) Bach, A.; Hutchison, J. M.; Holiday, R. J.; Crim, F. F. *J. Phys. Chem. A* **2003**, *107*, 10490. (c) Bach, A.; Hutchison, J. M.; Holiday, R. J.; Crim, F. F. *J. Chem. Phys.* **2002**, *116*, 9315.

amidogen are observed in the dc discharge with ammonia in the absence of Ba in the vapor, and the amidogen lines are not observed in the dc discharge in the presence of Ba vapor. The production of amidogen in the dc discharge suggests an alternative mechanism for the formation of products with these metals that leads to a natural explanation of the formation of the imide in reaction with Ba and the formation of amides in the reactions with Mg, Ca, and Sr. Figure 5 compares the potential energy surfaces for interactions of Ba and Sr atoms with amidogen, NH_2. In the case of the Ba atom, formation of the Ba−N bond releases essentially the same amount of energy as is required to dissociate another H atom from NH_2 to form BaNH. Internal thermal energies are sufficient to spontaneously dissociate the H atom from $BaNH_2$. This is not the case for the other metals, which remain in the potential energy well of MNH_2. The selectivity of product formation for these metals suggests that the dominant reaction mechanism in the dc discharge is direct reaction of the metal atoms with amidogen in the ground electronic states.

Conclusions

Millimeter-wave spectroscopy has shown that when barium reacts with ammonia in the gas phase, it produces barium imide, not the amide as expected from previous studies with Mg, Ca, and Sr. Barium imide was found to be linear with $r_{Ba-N} = 2.077$ Å and $r_{N-H} = 1.012$ Å. Electronic structure calculations confirm the linear structure and the importance of Ba−N π bonds. Although barium is formally classified as an alkaline earth metal, it has some properties similar to the transition metals. In the BaNH molecule, the Ba atom is in the formal +2 oxidation state, and the formal −2 charged imide ligand bonds to the Ba atom by two-electron donation from the filled nitrogen σ lone pair into the formally empty Ba 5d σ orbital. Also similar to the bonding with transition metals, multiple bond character develops by donation from the N 2pπ electron pairs into the formally empty Ba 5dπ orbitals and accounts for the linear structure. The availability of acceptor orbitals on the metals and donor orbitals on the nitrogen also accounts for the planar structures of the Mg-, Ca-, and Sr-amido molecules. The formation of these molecules from reaction of the metals with ammonia in the gas phase is accomplished apparently through the creation of the amidogen radical (NH_2) in a dc discharge, perhaps from excitation of NH_3 to the first singlet excited state or some alternative mechanism. The reaction of the Ba atom with amidogen continues on to the imido species, while reactions with the other metals remain at the amido species, because of the greater ease of oxidation of the Ba atom and the greater strength of the Ba−NH π bonds. Formation of the Ba−N triple bond in the Ba-imide species provides sufficient energy to oxidize the Ba atom and dissociate one of the N−H bonds of amidogen. Similar factors are likely at play in the bond-breaking and bond-making chemistries of N−H bonds with other metals.

Acknowledgment. The National Science Foundation, Grant CHE-0411551 (L.M.Z.) and Grant CHE0416004 (D.L.L.), and the donors of the American Chemical Society Petroleum Research Fund, Grant 41551−AC3 (D.L.L.), are gratefully acknowledged for support of this work. We also thank Carles Bo for providing the program to calculate the AIM atomic charges and Kittusamy Senthilkumar for helpful discussions on the fragment molecular orbital analysis.

JA053473K